Color-variable dual-dyed photodynamic antimicrobial polyethylene terephthalate (PET)/cotton blended fabrics

Chenyu Jiang[1] · Sarah Dejarnette[2,5] · Wangbingfei Chen[3] · Frank Scholle[2,5] · Qingqing Wang[3] ·
Reza A. Ghiladi[4,5]

Abstract

The urgent demand for scalable, potent, color variable, and comfortable antimicrobial textiles as personal protection equipment (PPE) to help reduce infection transmission in hospitals and healthcare facilities has significantly increased since the start of the COVID-19 pandemic. Here, we explored photodynamic antimicrobial polyethylene terephthalate/cotton (TC) blended fabrics comprised of photosensitizer-conjugated cotton fibers and polyethylene terephthalate (PET) fibers dyed with disperse dyes. A small library of TC blended fabrics was constructed wherein the PET fibers were embedded with traditional disperse dyes dominating the fabric color, thereby enabling variable color expression, while the cotton fibers were covalently coupled with the photosensitizer thionine acetate as the microbicidal agent. Physical (SEM, CLSM, TGA, XPS and mechanical strength) and colorimetric (K/S and *CIELab* values) characterization methods were employed to investigate the resultant fabrics, and photooxidation studies with DPBF demonstrated the ability of these materials to generate reactive oxygen species (i.e., singlet oxygen) upon visible light illumination. The best results demonstrated a photodynamic inactivation of 99.985% (~3.82 log unit reduction, $P = 0.0021$) against Gram-positive *S. aureus*, and detection limit inactivation (99.99%, 4 log unit reduction, $P \leq 0.0001$) against Gram-negative *E. coli* upon illumination with visible light (60 min; ~300 mW/cm^2; $\lambda \geq 420$ nm). Enveloped human coronavirus 229E showed a photodynamic susceptibility of ~99.99% inactivation after 60 min illumination (400–700 nm, 65 ± 5 mW/cm^2). The presence of the disperse dyes on the fabrics showed no significant effects on the aPDI results, and furthermore, appeared to provide the photosensitizer with some measure of protection from photobleaching, thus improving the photostability of the dual-dyed fabrics. Taken together, these results suggest the feasibility of low cost, scalable and color variable thionine-conjugated TC blended fabrics as potent self-disinfecting textiles.

Graphical abstract
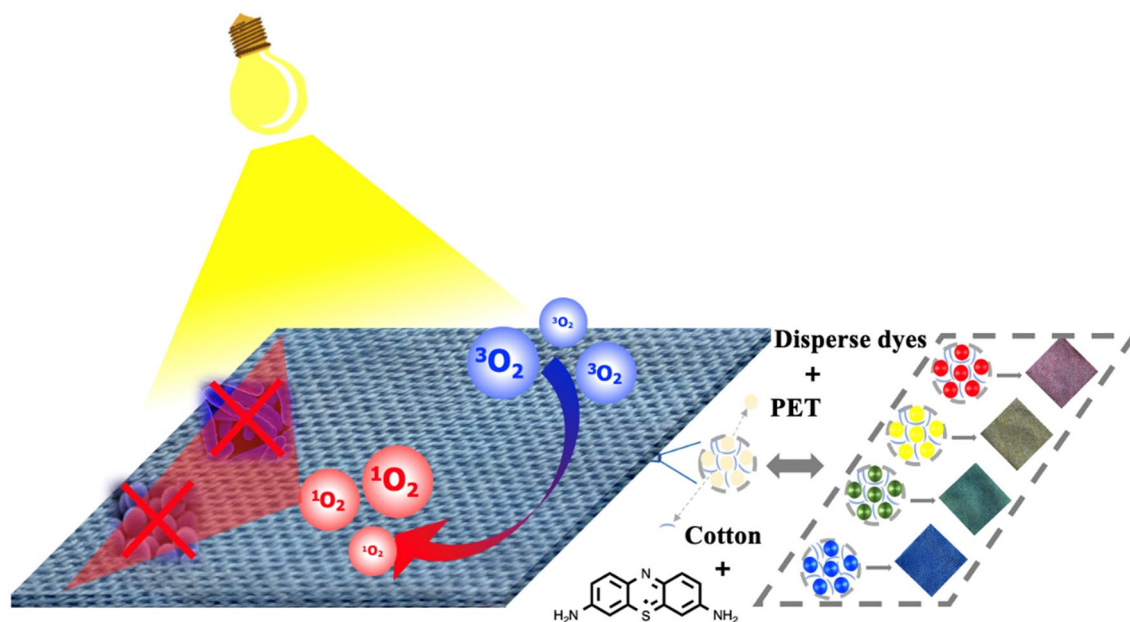
Keywords Antibacterial · Antiviral · Cotton · Photodynamic inactivation · Photostability · Textiles

1 Introduction

Hospital-acquired infections (HAIs) are a major threat to human health worldwide, responsible for 1.7 million infections and approximately 100,000 deaths annually, with a $45 billion economic burden in the US alone [1]. Since the start of the catastrophic COVID-19 pandemic caused by the SARS-CoV-2 virus, concerns over HAIs have increased as global health care systems have become overwhelmed with potentially infectious patients seeking testing and care [2]. Preventing the spread of HAIs to and from healthcare workers and patients heavily relies on the effective use of personal protective equipment (PPE), e.g., gloves, face masks, air-purifying filters and gowns [3]. However, current PPE can only physically prevent the direct exposure of the wearers to the microbial pathogens rather than inactivating them [4–6], leaving the pathogens potentially infectious on the PPE surfaces, thus increasing the risk of infections caused by cross-contamination or during the PPE removal process [6, 7]. To address these issues, many strategies have been explored for imparting antimicrobial properties to PPE, including embedding different bactericidal agents like antibiotics [8], quaternary ammonium salts [9], and metal nanoparticles [10], and although each of these strategies can be considered successful, they all exhibit one or more limitations including poor efficacy against drug-resistant pathogens [11],

inducing drug-resistance itself [12], environmental toxicity, and/or unacceptable side effects [13].

To circumvent some of the limitations associated with several of these antimicrobial strategies, antimicrobial photodynamic inactivation (aPDI) has been investigated as a promising strategy to produce nonspecific, robust, environmentally friendly and cost-effective antimicrobial materials. Photodynamic materials employ a nontoxic photosensitizer (PS), visible light, and molecular oxygen to generate reactive oxygen species (ROS), including hydroxyl radicals (OH), superoxide (O_2^-) and singlet oxygen ($^1O_2$), as bactericidal agents that cause irreversible damage to the bacterial cell membrane and/or cellular components leading to pathogen inactivation [14]. A number of potent photodynamic antimicrobial materials have been developed, including rose bengal and toluidine blue-O conjugated cellulose film [15], porphyrin-conjugated cellulose materials (nanocrystals, nanofibers, and paper) [16–21], BODIPY-conjugated paper sheets [19], PS-embedded polyacrylonitrile nanofibers [22, 23] or olefinic block copolymers [11], and PS-containing spray coatings [24, 25]. Among all the diverse applications for these photodynamic materials, self-disinfecting textiles are particularly attractive not only as their inherent wearable properties makes them ideal candidates for PPE, but also that their antimicrobial ability can eliminate odor and mildew stains caused by microorganisms [26], and prevent the excretion of acid by bacteria to protect against both discoloration and mechanical damage [27]. Materials based on an

aPDI strategy also have advantages for antimicrobial textiles as the short lifetime (87 ms for $^1O_2$ in CCl_4 solvent [28]) and limited diffusibility (55 nm for $^1O_2$ in tissue [29]) of the bactericidal ROS agents are not able to penetrate the stratum corneum, the outermost layer of the epidermis measuring 10–30 μm in thickness that is comprised of corneocytes (dead cells) [30], and is therefore considered safe for the user. Several photodynamic antimicrobial textiles employing photosensitizer-grafted cellulosic fabrics [31], polypropylene nonwoven fabrics [32], or polyester/cotton fabrics [33] have been successfully designed, however the appearance of these fabrics were dominated by the color of photosensitizer itself, and thus limited the commercial application of the these fabrics. To initially address this limitation, we designed a series of color-variable rose bengal embedded wool/acrylic blended fabrics [26, 27], and although these materials showed promise in terms of their tunable color palette and photodynamic efficacy, the inherent scratchy feel of wool and its poor heat dissipation limits the wearability of wool/acrylic fabrics as PPE. Moreover, these materials employed an electrostatic attachment of the anionic rose bengal photosensitizer to the cationic wool fibers, and this may be compromised during laundering.

To overcome these application and design limitations, here we chose to employ polyethylene terephthalate/cotton (TC) blended fabrics as the basis for a next-generation dual-dyed photodynamic textile. The TC blended fabric is one of the most comfortable and affordable fabrics on the market, combining the advantages of both cotton and PET textiles, such as breathability and good mechanical properties [34]. To prepare the color-variable photodynamic antimicrobial TC fabrics, the PET fibers were dyed with 4 different traditional disperse dyes (red, yellow, blue, green) using a traditional PET high-temperature high-pressure (HTHP) dyeing

method to tune the color of the fabrics, and the photosensitizer thionine was grafted onto the cotton fiber via covalent attachment using cyanuric chloride (2,4,6-trichloro-1,3,5-triazine) as the coupling agent (Fig. 1) [16, 35]. Thionine, a dye that is structurally related to methylene blue, has been shown to be a relatively low-cost, yet efficient photosensitizer, and, more importantly, thionine maintains its ability to photodynamically generate singlet oxygen even when grafted to a surface [36]. Physical (SEM, CLSM, TGA, XPS and mechanical property), colorimetric (K/S, *CIELab* values) and photooxidation studies against DPBF as a model substrate were employed to characterize the resultant small library of antimicrobial PET/cotton fabrics, and photodynamic inactivation studies employing both Gram-positive and Gram-negative bacteria were performed. Human coronavirus strain 229E (a BSL-2 surrogate for SARS-CoV-2) was employed as a model virus to investigate the antiviral activities of the prepared fabrics against enveloped viruses. The photostability of both single and dual-dyed fabrics under different light sources and environmental conditions was also investigated to assess if the disperse dyes could protect the thionine photosensitizer from photobleaching. Taken together, the results strongly suggest the feasibility of thionine-conjugated TC blended fabrics as high-performance, color-tunable self-disinfecting textiles.

2 Experimental

2.1 Materials

Polyester terephthalate/cotton blended yarns (abbreviated as TC) were obtained from Uster Technologies (Suzhou, China) Co., Ltd. Disperse red 153 (abbreviated as DR,

Fig. 1 The schematic illustration of the preparation of dual-dyed TC blended fabrics and their corresponding photographic images. Also shown are the photographs of the fabrics when dyed with either the disperse dyes or thionine alone
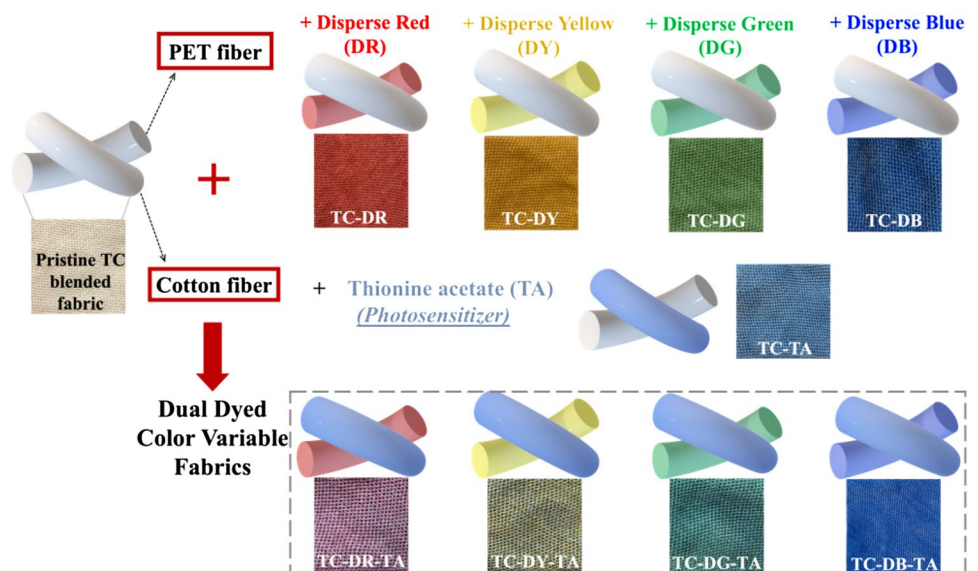
CAS: 78564-87-1), disperse yellow 23 (abbreviated as DY, CAS: 6250-23-3), and disperse blue 60 (abbreviated as DB, CAS: 12217-80-0) were purchased from Meiernuo Chemical Co. (Wenzhou, China). Disperse green dye (abbreviated as DG) was prepared by mixing DY and DB in 1:1 ratio. Sunsolt 7000 (CAS: 65423-83-8) was purchased from Nicca Chemical Technology Consultation (Shanghai, China) Co., Ltd. and was used as a dispersant during the dyeing process. Thionine acetate (CAS:78,338–22-4) was purchased from J&K Scientific (Beijing, China) Co., Ltd. 1,3-diphenylisobenzofuran (DPBF) was purchased from Shanghai Vita Chemical Reagent Co. Ltd. All other chemicals were of laboratory grade and used as received from commercial sources without further purification.

2.2 Preparation of antimicrobial fabrics

2.2.1 Polyester/cotton blended (TC) fabric

Polyester/cotton blended yarns were knitted into a plain knit structure on a CMS 530 HP knitwear flat knitting machine (STOLL, Germany) with a working width of 50″/127 cm.

2.2.2 High temperature–pressure polyester dyeing

Knitted TC fabric was cut into 8 cm × 8 cm swatches before being dyed in a high temperature–pressure dyeing machine (Datacolor, AHIBA IR, USA). Two 8 × 8 cm fabric swatches were dyed with 0.5% o.w.f. disperse dye (DR, DY, DG or DB) in 100 mL water and 10 mL dispersant under a continuous heating process of 4 °C/min from 30 to 130 °C, and maintained at 130 for 30 min. The dyed fabric was boiled in water (1:40 bath ratio) containing 2 g/L NaOH and 2 g/L $Na_2S_2O_4$ for 20 min to remove free dyes, polyester oligomers and other impurities, then washed with copious amounts of water and dried at 40 °C to improve the color fastness and vividness of the dyes.

2.2.3 Thionine-conjugated cotton yarns

Pristine TC fabric and the DR, DY, DG, or DB singly dyed T/C fabrics from Sect. 2.2.2 were separately soaked in 1 M NaOH over 1 h to deprotonate the hydroxyl groups of the cotton yarn. The alkalized fabric was then placed in a solution of cyanuric chloride (2,4,6-trichloro-1,3,5-triazine; variable concentration based on amount of thionine used in Table 1) in tetrahydrofuran and incubated for 12 h at 40 °C, after which deionized water and tetrahydrofuran were used to wash out unreacted cyanuric acid and other impurities. The activated fabric was then submerged in a solution of thionine acetate (TA; 0.25 molar equiv of cyanuric chloride) in 80 mL deionized (DI) water at 40 °C for another 12 h. The conjugated fabrics were first dried at 40 °C, and then

Table 1 Concentrations of thionine and cyanuric chloride used in the production of the TA-conjugated TC fabrics

TC-TA% (w.o.f.)	Amount of TA (mmol)	Amount of TCT (mmol)
0% (TC)	0	0
0.72% (TC-TA1)	0.125	0.5
1.44% (TC-TA2)	0.25	1
5.76% (TC-TA3)	1	4
11.52% (TC-TA4)	2	8

washed with deionized (DI) water and phosphate buffered saline (PBS; aqueous solution of 340 mM NaCl, 6.8 mM KCl, 20.0 mM Na_2HPO_4, 1.8 mM KH_2PO_4) to remove free thionine acetate. The washings were collected for calculating the amount of TA loaded onto the fabrics as follows: to ensure the successful removal of unbound thionine from the washing procedure, the prepared fabrics were placed into 3 mL PBS/cm^2 fabric for 1 h with vigorous shaking before being transferred to a cuvette and the absorbance at 603 nm, corresponding to the absorption maximum of thionine acetate, was recorded. When the leaching of TA could no longer be observed within the detection limit of the spectrometer, the fabrics were then dried at 40 °C in an oven and stored in the dark until further use. Different initial concentrations of TA were employed to explore the concentration-dependent bactericidal activity of TA, and the names and relative the amounts of TA used are listed in Table 1.

2.2.4 Photobleaching of thionine-conjugated antimicrobial fabrics

The thionine-conjugated TC-TA and the four dual-dyed TC-DR-TA, TC-DY-TA, TC-DG-TA and TC-DB-TA fabrics were cut into 3 cm × 3 cm swatches and then illuminated at a vertical distance of 15 cm for 12 h with a xenon lamp (500 W) equipped with a long-pass filter ($\lambda \geq 420$ nm), and these samples are referred to with the suffix 'B12h'. One control group of fabrics was similarly illuminated but under a humid environment with 1 mL water added to the fabric swatch every 2 h for 12 h, referred to with the suffix 'HB12h'. Another control group of fabrics was illuminated under a commercially available LED light (white light, 10 W) at a vertical distance of 18 cm for 5 days without any other light sources, and is referred with a suffix 'LED'.

2.3 Physical characterization

2.3.1 Determination of dye loading

The amount of loaded thionine acetate for each fabric (F, mol/g) was calculated based on an absorbance:concentration

relationship at the λ_{max} of the dyes (determined by the Beer-Lambert law) using the following Eq. 1:

$$F = \left(M_0 - C_1 V_1 - C_2 V_2\right)/W_f \tag{1}$$

where M_0 (mol) is the initial TA quantity added, C_1 (mol/L) and V_1 (L) are the concentration and volume of the collected water washings, and C_2 (mol/L) and V_2 (L) are the concentration and volume of the collected PBS washings, and W_f (g) is the weight fabric.

2.3.2 Photometry and colorimetric characteristics

The colorimetric characteristics [CIE (L*, a*, and b*) color space and color depth (K/S)] of the dual-dyed fabrics were evaluated using a Datacolor 650 spectrophotometer (USA) employing a D65 light source with an aperture of 9 mm. Each sample was folded into 2 layers to give a sufficient thickness to prevent show-through. The K/S values of the fabrics were calculated by the Kubelka − Munk equation (Eq. 2) as follows:

$$K/S = (1 - R)^2/2R \tag{2}$$

where K and S are the absorption and scattering coefficient of the fabrics, and R is the reflectance of the fabrics at λ_{max}. The spectra were normalized to the intensity of the 700 nm peak, except for the DG series that was normalized to the intensity of the 540 nm peak. K/S values have also been used, at the wavelength of maximum absorption, to gain a quantitative assessment of the amount of dye on fabric, with the degradation of thionine calculated based on the K/S values of unbleached fabrics vs. the corresponding bleached ones.

2.3.3 Confocal laser scanning microscopy (CLSM)

Confocal laser scanning microscopy was performed on a TCS SP8 instrument (Leica Microsystems GmbH, Germany) to visualize the localization of the disperse dyes and thionine acetate on the TC fabric. Laser excitation at 488 and 552 nm were employed to excite the disperse red (DR) dye and thionine acetate, respectively, with corresponding emission wavelengths of 570–630 (for DR) and 610–680 nm (for thionine acetate). The dual-dyed fabrics were first deconstructed by a knife to separate the yarns, which were then placed on a glass slide with one drop of water to smooth the surface, and then a coverslip was added on top, whose four edges were sealed with nail polish.

2.3.4 X-ray photoelectron spectroscopy (XPS)

The surface chemical compositions of one cotton fabric and TC-TA were characterized by X-ray Photoelectron Spectroscopy (Kratos Analytical Axis Ultra). The cotton fabric was fully washed by ethanol and DI water to remove any unbound species prior to characterization. All data were calibrated to the C–C peak at 284.8 eV.

2.3.5 Scanning electron microscopy (SEM)

The surface morphology of dye-free TC, TC-TA, and TC-DY-TA fabrics were visualized with a SU1510 (Hitachi, Ltd., Japan) scanning electron microscope with an accelerating voltage of 5.0 kV. Images were gathered at either of 500, 1000 or 5000 × magnification at room temperature. Prior to SEM imaging, the prepared samples were fixed on a metal plate by conductive resin and were sputtered with a thin layer of gold nanoparticles.

2.3.6 Synchronous thermal analyzer (STA)

Thermal gravimetric analysis (TGA) and differential scanning calorimetry (DSC) of the pristine TC, singly dyed TC-DY, and dual-dyed TC-DY-TA fabrics, as well as pure thionine acetate, were carried out using a thermal analyzer (Mettler, Toledo) under continuous N_2 purging (60 mL/min). Each sample (~5 mg) was heated in a platinum pan sample holder from 30 to 790 °C at a rate of 10 °C/min. Differential thermogravimetry (DTA) was deviated based on the TGA data.

2.3.7 Mechanical property studies

Bursting strength tests were employed to investigate the mechanical properties of TC, TC-DY, and TC-DY-TA fabrics via an electronic fabric strength tester from Hongda Experiment Instructions Co. Ltd (Nantong, China). Bursting strength values were determined by the constant-rate-of-traverse (CRT) ball burst method according to GB/T 19,976 (2005). Briefly, samples were cut into 80 mm diameter circles to cover the ring snare mechanism with an inner diameter of 45 mm. A polished steel ball with a diameter of 25 mm was pressed into the fabric sample through a ring snare mechanism at 300 mm/min. The force required for penetrating each sample was recorded.

2.3.8 UV–visible spectroscopy

The absorption spectra of saturated DR, DY, and DB acetone solutions were obtained on a Shimadzu UV-2600 UV–visible spectrophotometer. The DG solution was prepared by mixing saturated DY and DB solutions in a 1:1 v/v ratio. The data were normalized by the peak value of DR at 500 nm.

2.3.9 Detection of singlet oxygen ($^1O_2$)

1,3-diphenylisobenzofuran (DPBF), a colorimetric agent that reacts with singlet oxygen to produce a colorless product, was used to detect $^1O_2$ production. Fabric samples (3 cm × 3 cm) were first soaked with 10 mL ethanol for 30 min to remove any leachable thionine, and were then placed in the bottom of a 10 mL beaker containing 5 mL 150 mM DPBF solution in ethanol. The sample was illuminated by a handheld laser (532 nm, 85 ± 1 mW/cm^2; HTPOW Laser Limited) for 10 min, and the UV–visible spectrum of the solution was recorded every 2 min at 410 nm.

2.4 Antimicrobial photodynamic inactivation (aPDI)

2.4.1 Bacterial cell culture

Staphylococcus aureus (*S. aureus*) ATCC-6538 was cultured overnight at 37 °C in tryptic soy broth (TSB) in an orbital shaker (100–120 rpm). *Escherichia coli (E. coli)* 8099 and methicillin-resistant *S. aureus* (MRSA) (ATCC-44) were grown by the same procedure but substituting TSB with lysogeny broth (LB) and tryptic soy broth (TSB) with 5 mg/L tetracycline, respectively. Bacterial strains were grown to an initial concentration of 10^7–10^9 CFU (colony forming units)/mL. Cultures were pelleted via centrifugation (10,000 × g) for 10 min, the supernatant was decanted, and the bacteria were re-suspended in phosphate buffered saline (PBS; aqueous solution of 170 mM NaCl, 3.4 mM KCl, 10.0 mM Na$_2$HPO$_4$, 1.8 mM KH$_2$PO$_{4,}$ pH 7.2) containing 0.05% Tween-80.

2.4.2 Antibacterial photodynamic inactivation assays

Photodynamic inactivation studies employing the above bacteria were performed in triplicate as previously described [24, 25, 27, 35, 37]. Briefly, three fabric samples (1 × 1 cm, ~40 mg) were individually placed into adjacent wells of two identically prepared 24-well plates. A 100 µL PBS aliquot containing 10^7–10^9 CFU/mL of bacteria was added to each of the three wells per plate. The 24-well plate was illuminated at a distance of 12 cm for a defined time period with a xenon lamp (500 W) equipped with a long-pass filter ($\lambda \geq 420$ nm) to provide a light fluence of ~ 65 ± 5 mW/cm^2, while an identically prepared 24-well plate was kept without illumination as the dark control. Following illumination, 0.9 mL of sterile PBS was added to each well in both the illuminated and the dark control plates, and the plates were manually stirred with a pipet for 10 s to resuspend the bacteria. Each sample well was then 1:10 serially diluted (100 µL in 0.9 mL aliquots of PBS) six times, and 10 µL from each diluted well were separately plated in columns on gridded six column square plates (TS-agar for *S. aureus* and MRSA;

LB-agar for *E. coli*), followed by overnight dark incubation at 37 °C. A material-free dark control was prepared by aliquotting 100 µL bacterial PBS solution into 0.9 mL sterile PBS, and following the same dilution process. The number of visible colonies on the agar plates was determined by colony counting, and the survival rate was determined by the ratio of CFU/mL of the illuminated plate versus that of the corresponding material-free dark control. The minimum detection limit was 10 CFU/well (based on the plated 10 µL aliquot from the 1 mL undiluted well), and the detection limits of bacterial survival for *S. aureus* and *E. coli* were 0.001% and 0.01%, respectively.

### 2.4.3 Antiviral photodynamic inactivation assays

Human coronavirus HCoV-229E was grown to a titer of 10^7 TCID$_{50}$/mL on the human hepatocarcinoma Huh-7 cell line in cell growth media (DMEM, 1% antibiotics, 10% fetal bovine serum, FBS) at 35 °C. The fabric samples (6 mm diameter) were fitted into the well-bottoms of a 96-well plate, and 25 µL of virus suspension (free of the host Huh-7 cells) was added to the wells. A set of dark controls wrapped in aluminum foil was left unexposed to light for 60 min. For samples exposed to light, the illumination conditions were 400–700 nm, 65 ± 5 mW/cm^2. After illumination for 60 min, 75 µL of infection media (DMEM 1% antibiotics, 1% FBS, 1% HEPES buffer) were added, and the virus was eluted by triturating several times, followed by rapid transfer to new wells. Virus suspensions were immediately diluted serially tenfold, and 50 µL of four replicates of each dilution were used to infect Huh-7 cells seeded the previous day at a density of 10^4 cells per well in a TCID$_{50}$ assay protocol. The plates were incubated at 35 °C with 5% CO$_2$. After 168 h, the cytopathic effect was monitored by visual inspection, and resulting log$_{10}$TCID$_{50}$/mL values (MDL of 2.8 log$_{10}$TCID$_{50}$/mL) were calculated according to the Spearman-Kaerber method. All studies were performed in triplicate.

# 3 Results and discussion

3.1 Material characterization

3.1.1 Materials preparation

The color-variable photodynamic antimicrobial TC fabrics were prepared in a two-step process wherein the PET fibers were dyed with 4 different common disperse dyes (red, yellow, blue, green) using a traditional PET high-temperature high-pressure (HTHP) dyeing method to tune the color of the fabrics (as illustrated in Scheme 1), and the photosensitizer thionine was grafted onto the cotton fiber via covalent attachment using cyanuric chloride (2,4,6-trichloro-1,3,5-triazine)
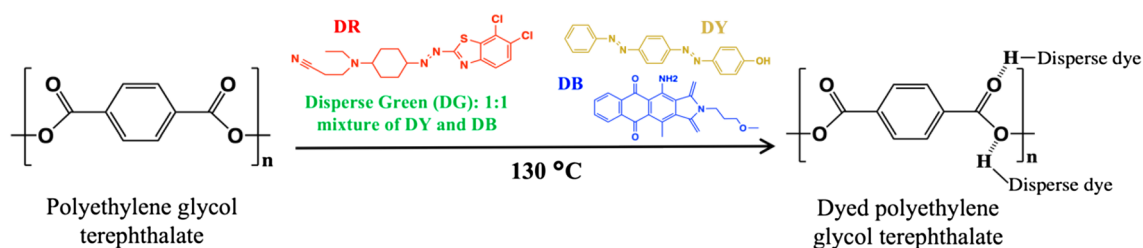
Scheme 1 Dyeing of polyethylene terephthalate fibers with disperse dyes
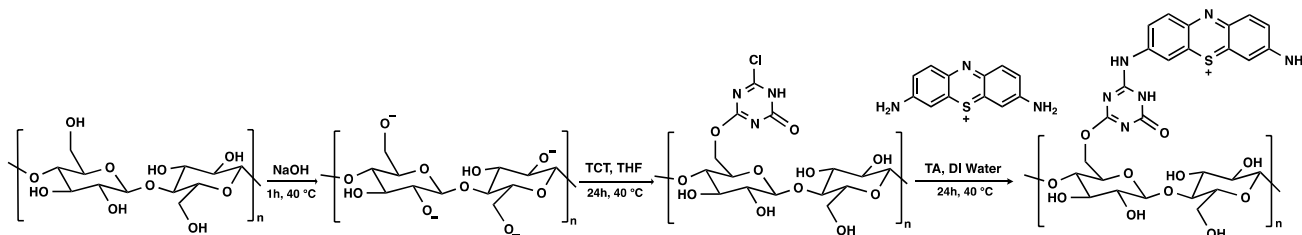
Scheme 2 The grafting of thionine onto cotton fibers via 2,4,6-trichloro-1,3,5-triazine coupling

as the coupling agent (Scheme 2). In HTHP dyeing, under high temperature and high pressure, the highly hydrophobic disperse dyes are able to penetrate the boundary layer of the PET fibers, where they are retained uniformly in the presence of a dispersant. Conversely, the hydrophilic cotton fibers are barely dyed with disperse dyes under these conditions [38], leaving the primary and secondary hydroxyl groups on the repeating units of the cotton fibers chemically reactive for surface modification via cyanuric chloride (2,4,6-trichloro-1,3,5-triazine) coupling, a method that has been previously successful in grafting photosensitizers onto cellulosic materials [16, 35, 39].

The physical appearance of the pristine PET/cotton (TC) blended fabric, the single-dyed thionine TC-TA fabric, the single-dyed disperse dye fabrics TC-DR, TC-DY, TC-DG and TC-DB, and the dual-dyed TC-DR-TA, TC-DY-TA, TC-DG-TA, and TC-DB-TA fabrics are displayed in Fig. 1. Compared to the pristine TC fabric, single-dyed fabrics via both HTHP (disperse dyes) and chemical conjugation (thionine) both presented with vivid colors as expected from the presence of the loaded dyes, with dual-dyed fabrics exhibiting colors that were the colorimetric combination of the disperse dyes with thionine. Notably, both HTHP and chemical conjugation resulted in a uniform material color, and no obvious variation in the physical touch or feel of the materials was observed for the dyed fabrics. This straightforward color change suggested the successful loading of both disperse dyes and thionine, and quantitative analysis of the loaded thionine onto the pristine and dyed fabrics was determined by differential uptake measurements comparing the amount of initially added thionine against that

Table 2 Loading of thionine acetate (mol/g) on the TC-TA, TC-DR-TA, TC-DY-TA, TC- DG-TA and TC-DB-TA fabrics, and the corresponding loading efficiency compared to the initial amount of thionine acetate

	TA loading (µmol/g)	Efficiency (%)
TC-TA	33.36	66.72
TC-DR-TA	22.75	45.50
TC-DY-TA	20.5	41.00
TC-DG-TA	23.25	46.50
TC-DB-TA	23	46.00

remaining in the residual bath after dyeing, as well as the amount recovered after each washing step. As shown in Table 2, single-dyed thionine possessed the highest loading amount of 33.36 µmol/g, representing 66.7% uptake of the initial thionine added in the conjugation process. All dual-dyed fabrics exhibited virtually the same level of loaded thionine (20.5–23.25 mol/g), representing a decrease in PS loading efficiency compared to the single-dyed TC-TA. The lower loading of thionine in the dual-dyed fabrics may be caused by the loss of reactive hydroxyl groups from a minor amount of surface damage to the cotton fibers during the HTHP process, which was shown by the micro-morphology observation studies (see below).

FT-IR spectroscopy was initially chosen to investigate covalent bond formation in the TC-TA materials, however, due to the low degree of substitution, no significant changes were observed (data not shown). Rather, we employed X-ray photoelectron spectroscopy (XPS) to confirm the covalent attachment of the PS in TC-TA (Fig. 2). As shown in Fig. 2a,
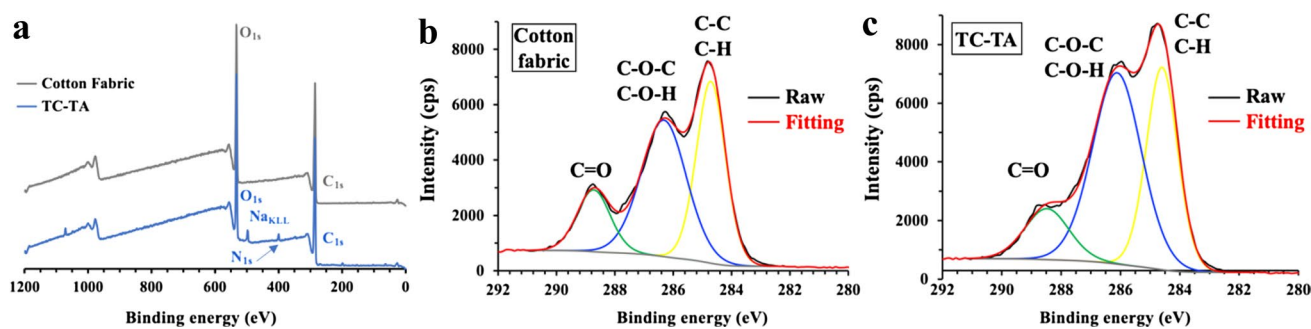
Fig. 2 The XPS survey scan spectra of (**a**) cotton fabric and TC-TA, and the C_{1s} XPS spectra and corresponding fittings of (**b**) cotton fabric and (**c**) TC-TA

the surface of the pristine cotton fabric was dominated by C_{1s} and O_{1s} signals, while new peaks corresponding to Na_{KKL} and N_{1s} from thionine were observed on the surface of the TC-TA, along with the C_{1s} and O_{1s} signals. This further demonstrated that thionine was successfully incorporated onto the surface of the fabric. As depicted in Fig. 2b, c, the C_{1s} curve of the pristine cotton fabric exhibited three peaks at 284.9, 286.6 and 288.1 eV, which corresponded to the C–C (or C-H), C–O–C (or C–O–H), and C=O signals, respectively. The peak at 286.6 eV and assigned as a C=O signal may be assigned to semi-cellulose or other impurities, which is consistent with previous literature reports [40, 41]. Similar peaks corresponding to C–C (or C-H), C–O–C (or C–O–H), and C=O were also observed in the C_{1s} curve of TC-TA, while the ratio, calculated on the relative distributions of the different bound carbons as estimated from the high-resolution carbon C_{1s} XPS spectra through the use of peak fitting to isolate the signals into different Gaussian components, of C–O–C increased from 45.66% to 52.13%. Considering the blending of PET fibers will not introduce a higher ratio of C–O–C bond [42], this increasing ratio was attributed to the C–O–C covalent bond between the cotton fiber and thionine.

3.1.2 Determination of thionine localization

TC-DR and TC-DR-TA fabrics were chosen as models to visualize the localization of the disperse dyes and thionine acetate via confocal laser scanning microscopy (CLSM), as the absorption and emission of DR and thionine are the easiest to distinguish when compared to the other disperse dyes. Both single PET fibers with straight cylinder structures and single twisted tube-like cotton fibers [34] were observed in all images (Fig. 3). Under bright field conditions (panels a, d, and g), the polyester fibers were opaque and dark in color for TC-DR and TC-DR-TA, whereas they appeared transparent for the untreated PET fiber in TC-TA, suggesting the loading of disperse red was mainly localized to the PET fibers. Consistent with the bright field images, in

merged panel b, the PET fibers in TC-DR showed a strong florescence signal from 570 to 630 nm (red) corresponding to the emission of DR, while the cotton fibers only presented a weak florescence signal, again indicating that the DR dye was mainly localized to the PET fibers. In panel e, the luminescence signal from 610 to 680 nm (green), attributed to thionine acetate, was observed only from the cotton fibers of the TC-TA fabric, indicating the localization of thionine was mainly on the cotton fibers (as designed). In panel h, the PET fibers showed a dark yellow color that can be considered as a combination of red and green signals given that DR has an absorption at both 488 and 552 nm excitation wavelengths (with emission observed in both the 570–630 nm and 610–680 nm windows), while the cotton fibers only exhibited a green signal from thionine, with the luminescence images (panel i) further demonstrating that. Taken together, the CLSM studies confirmed the loading of the disperse dyes and thionine on the dual-dyed fabrics, and, more importantly, demonstrated their localization to the PET and cotton fibers, respectively, as designed.

3.1.3 Colorimetric characterization of the fabrics

CIELab color values [light–dark (L*), red-green (a*), and yellow-blue (b*)] of the pristine TC, single and dual-dyed fabrics are provided in Table 3, and their corresponding color space coordinates are shown in Fig. 4. The coordinates of the thionine-only single-dyed TC-TA were observed closer to the yellow-blue (b*) axes, with a small a* value of − 2.2 and a large b* value of − 15.4, consistent with the cyan color of the thionine-only TC-TA fabric in Fig. 1. As expected, compared to pristine TC and disperse dye single-dyed fabrics, the b* value of thionine-loaded fabrics showed an obvious decrease corresponding to the hypsochromic color shift of the fabrics. The yellow (TC-DY and TC-DY-TA) and blue (TC-DB and TC-DB-TA) series fabrics exhibited the greatest (-38.11) and least (-4.4) change in b* value, respectively, representing the most and least color change due to the loading of thionine. Overall, the coordinates of
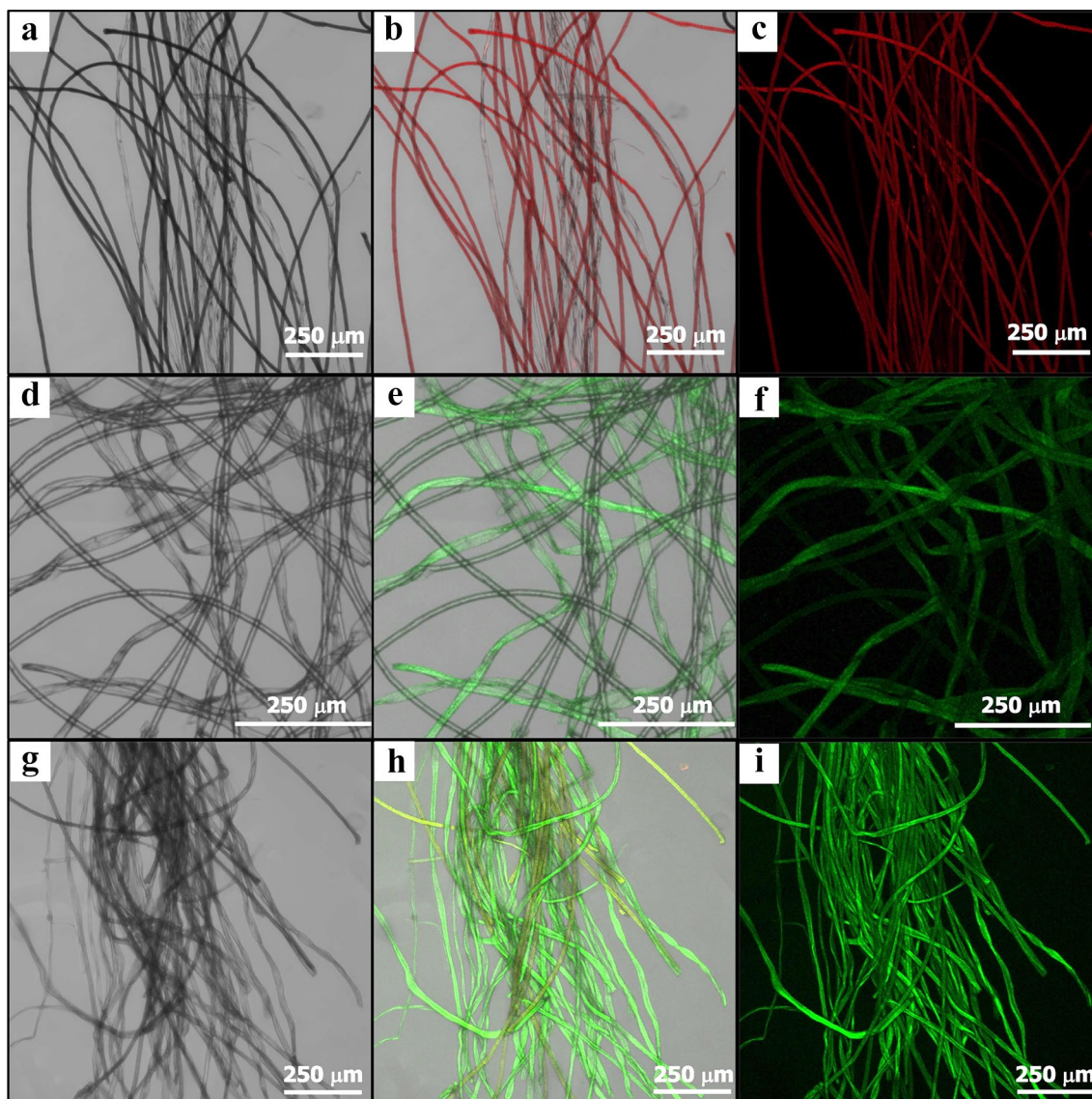
Fig. 3 CLSM images of TC-DR (**a–c**), TC-TA (**d–f**) and TC-DR-TA (**d–f**). Panels **a**, **d**, and **g** are bright-field images, panels **c** ($\lambda_{ex} = 488$ nm; $\lambda_{em} = 570–630$ nm), **f** ($\lambda_{ex} = 552$ nm; $\lambda_{em} = 610–$ 680 nm), and **i** ($\lambda_{ex} = 488$ nm; $\lambda_{em} = 570–630$ nm) are luminescence images, and panels **b**, **e**, and **h** are the merged images

Table 3 *CIELab* values of the pristine TC and single-dyed TC-DR, TC-DY, TC-DG, and TC-DB fabrics (− TA), and the corresponding fabrics dyed with thionine (+TA)

	L*		a*		b*	
	N/TA	+ TA	N/TA	+ TA	N/TA	+ TA
TC	90.23	63.79	− 0.01	− 2.22	7.6	− 15.43
TC-DR	56.05	44.39	41.27	17.94	18.89	1.28
TC-DY	74.31	50.86	17.29	− 4.87	47.89	9.78
TC-DG	63.31	48.04	− 18.57	− 13.06	16.31	2.99
TC-DB	49.06	43.67	0.83	1.3	− 25.89	− 30.29

TC-TA were found in the green–blue (− a*, − b*) quadrant, the coordinates of the dual-dyed fabrics were found in the red-yellow (+ a*, + b*) quadrant for TC-DR-TA, the green-yellow (− a*, + b*) quadrant for TC-DY-TA and TC-DG-TA, and the red-blue quadrant (+ a*, − b*) for TC-DB-TA, which essentially followed the coordinates of the
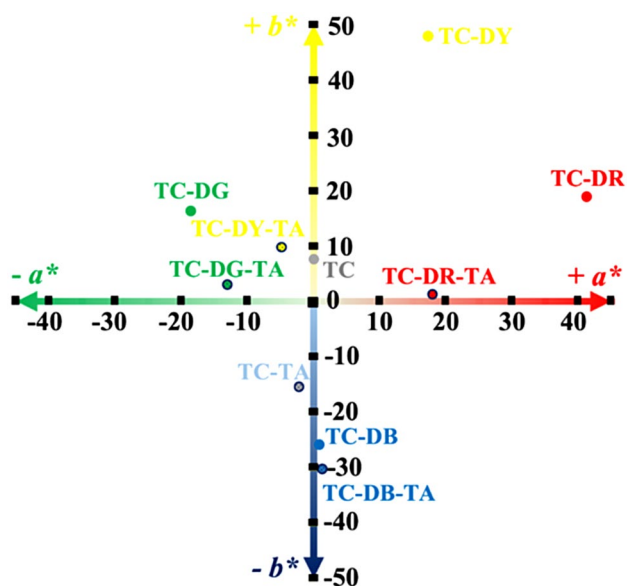
Fig. 4 The coordinate positions of TC-TA, TC-DR-TA, TC-DY-TA, TC-DG-TA, and TC-DB-TA fabrics in *CIELab* color space for a* and b*. The L* values were not plotted for simplicity

disperse dye single-dyed fabrics, suggesting that although the colors of the dual-dyed fabrics resulted from a colorimetric combination of the disperse dyes and thionine, the dispersed dyes were the ones that dominated the fabric colors.

Color depth (K/S value) characterization (reflectance measurements) was also performed on the fabrics. The UV–visible absorption spectra of the DR, DY, DG and DB disperse dyes in acetone solution, as well as TA in aqueous solution, are shown in Figure S1. As shown in Fig. 5a, the TA single-dyed fabrics all presented one characteristic peak around 610 nm, which is consistent with the characteristic

absorption peak of aqueous thionine. Furthermore, as expected for thionine as a dye, the intensity of this characteristic peak proportionally increased as the amount of thionine used in the dyeing process increased from 0.125 mmol (TC-TA1) to 2 mmol (TC-TA4). Meanwhile, single-dyed TC-DR, TC-DY, TC-DG, and TC-DB (solid lines in Fig. 5b) exhibited absorption maxima 500, 450, 660, and 670 nm, respectively, consistent with the characteristic absorptions of the disperse dyes in acetone solution (Figure S1), which further provides evidence for the presence of the disperse dyes on the fabrics. Dual-dyed fabrics TC-DR-TA, TC-DY-TA and TC-DG-TA (dotted lines in Fig. 5b) exhibited characteristic peaks from both the corresponding disperse dye and the thionine photosensitizer, while TC-DB-TA appeared to only have one peak centered around 620 nm, which is likely attributable to the overlap of the DB and TA absorption maxima. The almost twofold stronger intensity of the 620 nm band of the dual-dyed fabric compared to the DB-only single-dyed fabric also supports this supposition. The colorimetric descriptions here provide a semi-quantitative analysis of the color changes of the dual-dyed TC fabrics, and suggest the successful loading of both thionine and disperse dyes on the fabrics.

3.1.4 Micro-morphology of the dyed fabrics

The morphological features of pristine TC, TC-TA, and TC-DY-TA fabrics were investigated by scanning electron microscopy. Artificial polyester (polyethylene terephthalate) fibers with a uniformly straight cylinder shape and natural cotton fibers with typical convolutions and kidney-shaped structures can be observed in the yarns of all 3 samples under lower magnification in Fig. 6a, c, and e). Panels b, d, and f show the higher magnification images, and the surfaces
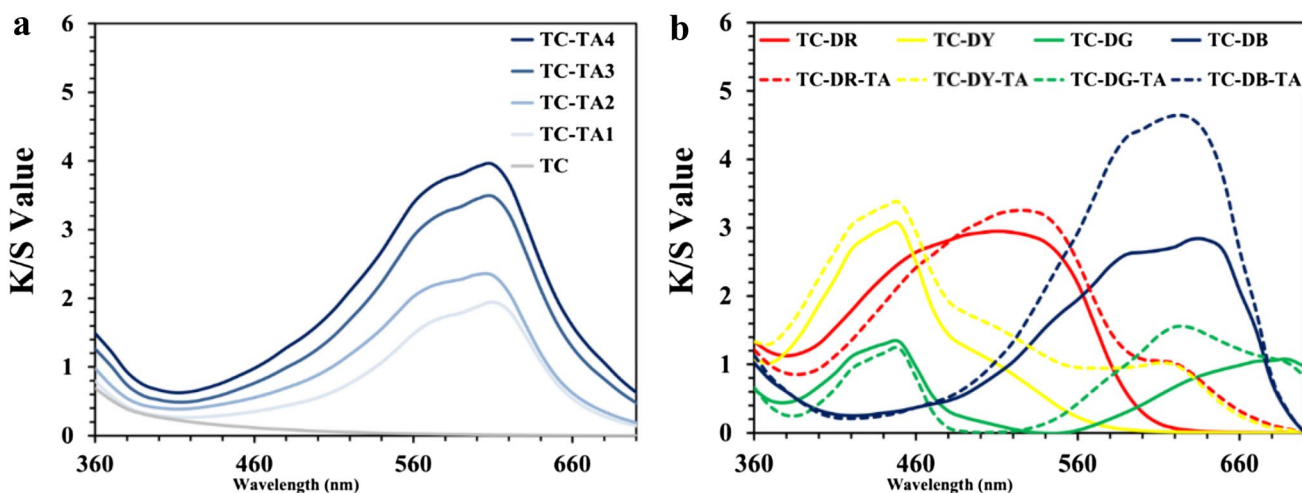

Fig. 5 Color depth (K/S) spectra of the thionine single-dyed fabrics (**a**), and disperse dye single-dyed fabrics (solid line) and dual-dyed fabrics (dotted-line) (**b**)
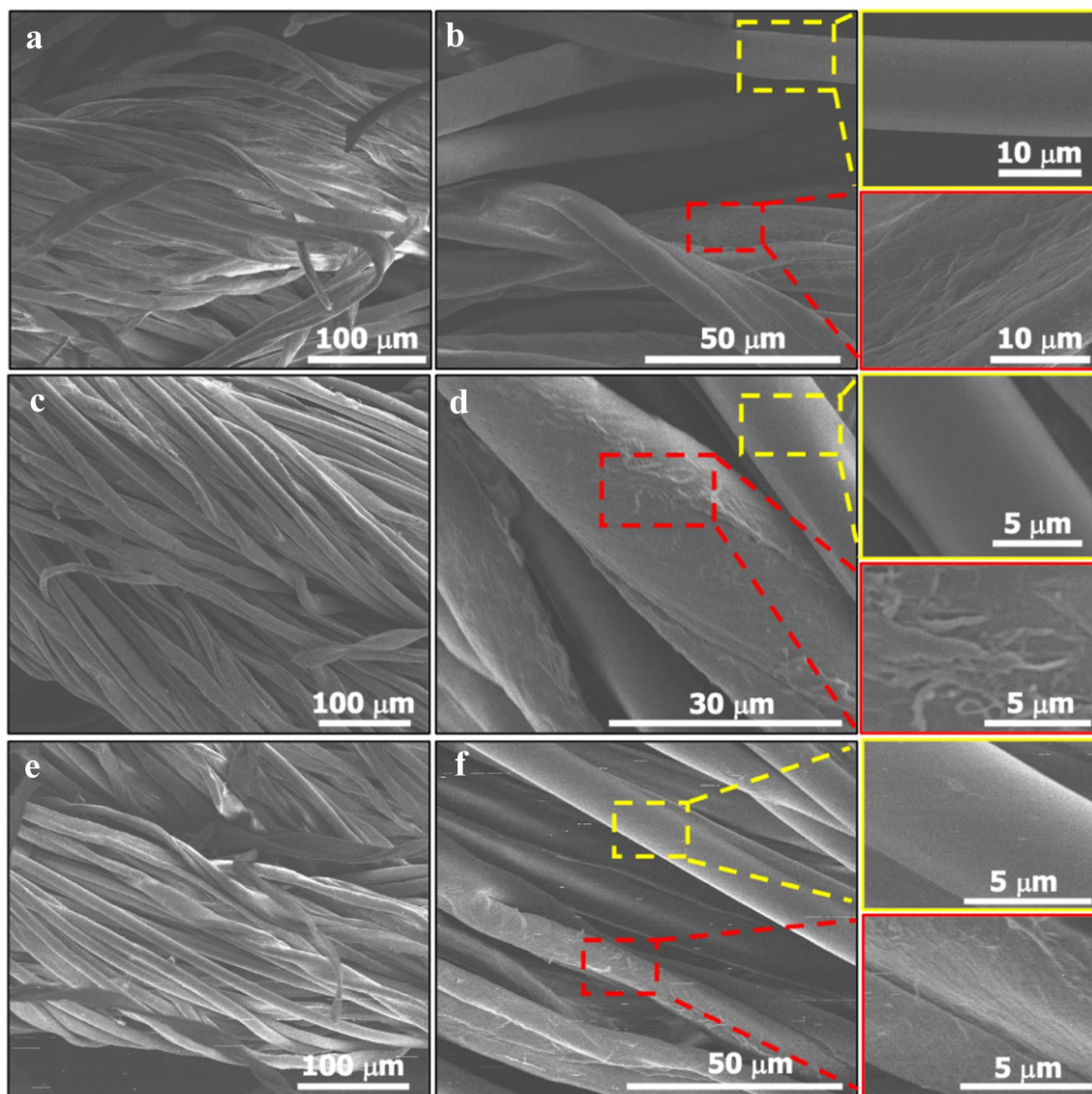
Fig. 6 SEM images of pristine TC fabric (**a**, **b**), TC-TA (**c**, **d**), and TC-DY-TA (**e**, **f**) under different magnifications ($\times$ 500 for **a**, **c**, and **e**; $\times$ 1000 for **b**, **d**, and **f**). Yellow and red outlined panels are higher magnification images ($\times$ 5000)

of the PET and cotton fibers are clearly visualized in the yellow outlined and red outlined panels, respectively. The PET fibers in the pristine TC, single-dyed TC-TA, and dual-dyed TC-DY-TA fabrics have no distinguishable features, with all fibers exhibiting smooth surfaces ($<$ 10 μm diameter), while the cotton fibers in the three samples show different surface features: for the cotton fibers from pristine TC fabric (panel b), some smooth grooves can be observed corresponding to the wax layer on the cuticle, the outermost layer of cotton fibers [43]. In the thionine single-dyed TC-TA fabric, a crisscross pattern owing to the non-structural orientation of cellulose and non-cellulosic materials from the primary walls (the secondary layer of cotton fibers [43]) can be clearly observed, indicating minor surface damage resulting from

the triazine coupling reaction. After both the high temperature–pressure dyeing and the coupling reaction, the cotton fibers in TC-DY-TA presented a compact parallel structure corresponding to highly ordered crystalline cellulose, which is only found in the inner secondary wall of cotton fibers, suggesting further damage to the cotton fiber surface that was attributed to the harsher two-step dyeing/coupling process employed for making the dual-dyed fabrics.

3.1.5 Thermal gravimetric analysis (TGA)

Thermal gravimetric analysis (TGA) under inert atmosphere was employed to understand the thermal behavior of pristine TC, single-dyed TC-DY, and dual-dyed TC-DY-TA fabrics.

As shown in the Fig. 7a, pristine TC exhibited three stepwise decomposition stages: in the first stage up to 100 °C, a minor initial weight loss of ~ 3% was noted, corresponding to the loss of moisture. A fast weight reduction (from ca. 97% to ca. 20%) was observed in a second stage with onset temperatures from 270 to 430 °C, attributed to the decarboxylation and dehydration of the fabric to volatile gasses or chars. Two DTG peaks around 340 °C and 420 °C for the pristine TC fabric were noted (Fig. 7b) in this stage, which are associated with the pyrolysis temperature of pure polyester [44] and cotton [45], respectively. A gradual weight decomposition from 20 to 0% with a maximal decomposition rate peak around 440 °C was further observed, indicating the decomposition of previously formed char and volatiles from the second stage was occurring during this final stage [46]. TC-DY and TC-DY-TA fabrics showed a comparable three stage decomposition profile as the pristine TC fabric. However, the onset temperature for the second stage of TC-DY (310 °C) and TC-DY-TA (320 °C) were both higher than that of the pristine TC fabric, suggesting both hydrogen bond and intra-strand cross-linking [16] formed during dyeing and conjugation processes, respectively, likely had a thermal stabilizing effect on the fabrics. In the third stage, compared to

the pristine TC fabric, both TC-DY, and TC-DY-TA fabrics displayed a more modest weight decomposition, from ca. 20% to ca. 10%, indicating a successful chemical modification of the raw TC material [45]. Overall, the TGA data suggest that both HTHP dyeing and triazine coupling do not negatively affect the thermal decomposition behavior of the TC fabric.

3.1.6 Mechanical property studies

To evaluate the damage caused by HTHP dyeing and the covalent attachment of thionine on the mechanical properties of the dyed materials, we employed bursting strength tests on TC, TC-DY and TC-DY-TA fabrics. As expected, pristine TC possessed the best mechanical property, with a bursting strength of 767 N. TC-DY was slightly lower at 727 N, while TC-DY-TA had the lowest value at burst of 681 N. The decreasing trend of bursting strength indicated that both HTHP dyeing and chemical conjugation via triazine coupling slightly altered the structure of the fabrics, which is consistent with the SEM observations. However, such decreases can still be considered minor, with the dual-dyed TC-DY-TA fabric still possessing a relatively fair mechanical burst strength for textile-based materials.

3.1.7 Determination of singlet oxygen production

1,3-diphenylisobenzo-furan (DPBF), a colorimetric chemical scavenger that exhibits a highly specific oxidative reaction with singlet oxygen ($^1O_2$) to form colorless 1,2-dibenzoylbenzene [47], was employed to determine $^1O_2$ generation by the fabrics. The UV–visible absorption spectrum of DPBF solution in the presence of the illuminated fabrics was monitored as a function of time. Initially, the DPBF ethanol solution with the TC-TA material exhibited a characteristic absorption maximum at 400 nm (Fig. 8a), which decreased linearly as a function of illumination time, suggesting the formation of singlet $^1O_2$. Similar spectral changes at 400 nm were also observed for the DPBF solution with TC-DR-TA, TC-DY-TA, TC-DG-TA and TC-DB-TA (Fig. 8b), suggesting that all thionine-containing single/dual-dyed fabrics could generate $^1O_2$ under visible light illumination. Negligible absorbance decreases at 400 nm were observed for the material-free light control (Fig. 8b) and material-present dark control (Fig. 8c), indicating that the photodynamic material and light were both necessary for the formation of $^1O_2$. These results provide unequivocal evidence for the generation of $^1O_2$ under visible light illumination for the TC-TA, TC-DR-TA, TC-DY-TA, TC-DG-TA and TC-DB-TA fabrics. Although these data cannot rule out other reactive oxygen species produced via a Type I photochemical mechanism, they demonstrated the ability of these fabrics
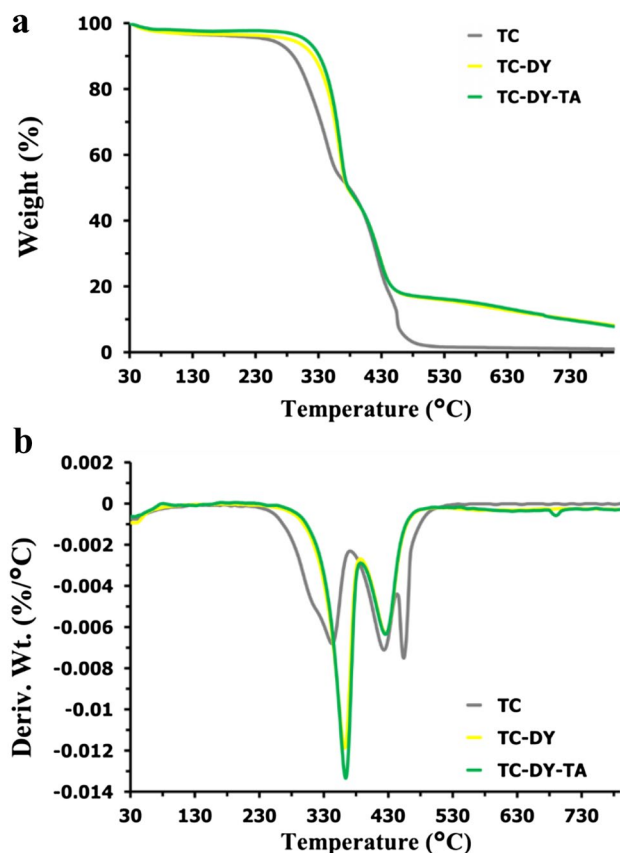

Fig. 7 TGA (**a**) and DTG (**b**) curves of pristine T/C fabric (gray), TC-DY (yellow), TC-DY-TA (green)
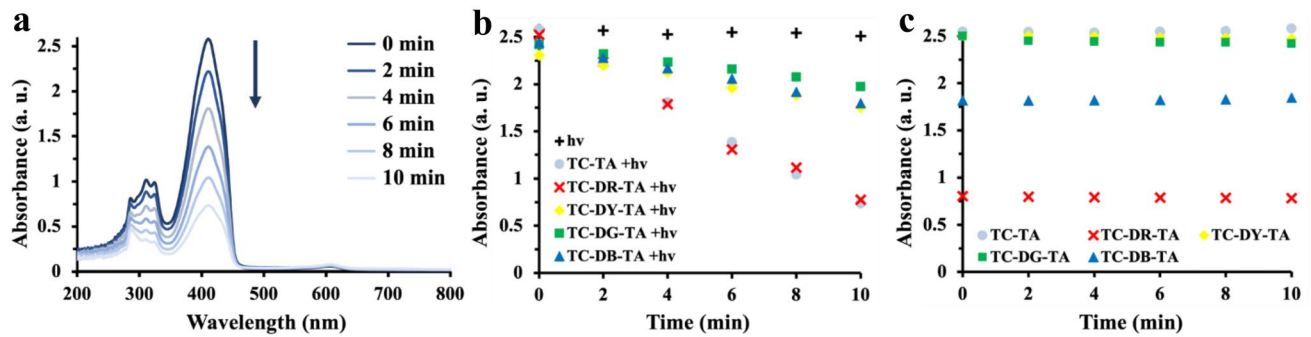
Fig. 8 Absorption spectra of the DPBF solution in the presence of TC-TA fabric under 532 nm laser illumination (**a**), the single wavelength data (400 nm) for studies performed with TC-TA, TC-DR-TA, TC-DY-TA, TC-DG-TA and TC-DG-TA fabrics as well as a material-free DPBF solution with (**b**) and without (**c**) illumination

to at least function via a Type II photochemical mechanism for pathogen inactivation [48].

3.2 Antimicrobial photodynamic inactivation studies

3.2.1 Photodynamic antibacterial activity of thionine single dyed-fabrics

In vitro aPDI studies against methicillin-resistant *S. aureus* (MRSA; ATCC-44) employing a series of thionine-loaded single-dyed fabrics with different amounts of thionine used in the coupling reactions were performed to determine the optimum thionine concentration to use for the dual-dyed materials. Unless otherwise noted, assays were carried out under fixed illumination conditions (60 min, 400–700 nm noncoherent light, 65 ± 5 mW/cm^2) and employed a starting concentration of 10^8–10^9 CFU/ mL determined by colony counting. As shown in Fig. 9, all dark control samples exhibited negligible inactivation without illumination, indicating the necessity for light to photodynamically generate biocidal ROS (consistent with the DPBF studies above). At the lowest level of thionine-loading (0.025 mmol/g), illumination of TC-TA1 resulted in MRSA inactivation of 99.86% (2.85 log units, $P = 0.0054$), and increased further to 99.99% (4 log units, $P = 0.0096$) at 0.05 mmol thionine/g TC-TA2. However, when the initial concentration of TA increased to 0.2 mmol/g (TA-TC3) and 0.4 mmol/g (TA-TC4), the inactivation efficacy decreased to 2.49 log units (99.68% inactivation, $P = 0.028$) and 1.59 log units (97.42%, $P = 0.0008$), respectively. One possible explanation for these counter-intuitive results at high thionine loadings (where greater pathogen inactivation was expected) is that the aggregation of thionine is substantially increased on the cotton surface, leading to photosensitizer self-quenching, which has been observed for the related photosensitizer methylene blue [49]. Such self-aggregation leads to fast non-radiative
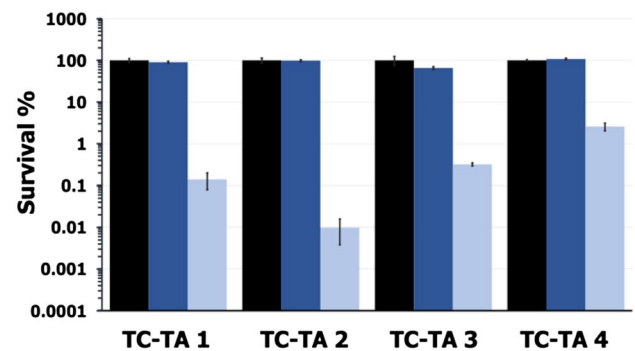

Fig. 9 Photodynamic inactivation studies employing TC-TA1-4 against MRSA (ATCC-44). Displayed are the % survival (*vs* material-free dark control, black) for the TC-TA1-4 dark controls (dark blue) and illuminated TC-TA1-4 materials (light blue). Illumination conditions are the same for all inactivation studies (60 min, 400–700 nm non-coherent light, 65 ± 5 mW/cm^2). The detection limit for MRSA here was 0.0001%

decay (3–4 ps) of excited dimer/aggregate photosensitizer [50], decreasing singlet oxygen production [51], and thereby negatively affecting the bactericidal efficacy of the fabrics. Given the results from these antimicrobial photodynamic inactivation studies, a loading of 0.05 mmol thionine/g fabric was used in the preparation of the dual-dyed fabrics.

3.2.2 Photodynamic antibacterial activity of TA and dual-dyed TC fabrics

Gram-positive *Staphylococcus aureus* (*S. aureus*) ATCC-6538 and Gram-negative *Escherichia coli (E. coli)* 8099 were employed to evaluate the in vitro inactivation efficacy of the dual-dyed fabrics. Unless otherwise noted, assays were carried out under fixed illumination conditions [xenon lamp (500 W) equipped with a long-pass filter ($\lambda \geq 420$ nm)] for 60 min and employed a starting concentration of 10^8–10^9 CFU/ mL for *S. aureus* and 10^7–10^8 CFU/ mL for *E.*

coli. Consistent with the above dark control results against MRSA, no significant inactivation was observed for either *S. aureus* or *E. coli* in the absence of light (Fig. 10), yet both bacteria exhibited population reductions in the presence of the photodynamic fabrics under visible light illumination. For *S. aureus* (Fig. 10 a), compared to the single-dyed TC-TA fabric that showed 99.98% inactivation (3.74 log units, $P = 0.088$) after 60 min illumination, the dual-dyed TC-DR-TA (99.91%, 3.04 log units, $P \leq 0.0001$) and TC-DB-TA (99.95%, 3.28 log units, $P = 0.0089$) exhibited slightly lower levels of inactivation, while TC-DY-TA ($P \leq 0.0001$) and TC-DG-TA ($P = 0.0021$) showed almost the same level of bactericidal efficacy (99.98%, 3.9 log units). These data demonstrate that the presence of the disperse dyes on the PET fibers had a limited impact on the ability of the thionine-loaded cotton fibers to mediate the photodynamic inactivation of *S. aureus*. A more obvious effect was noted for *E. coli*: for TC-TA and TC-DB-TA, detection limit inactivation (99.99%, 4 log units, both $P \leq 0.0001$) was observed. For

TC-DR-TA and TC-DG-TA, similar inactivation levels of 99.9% (3 log units, $P \leq 0.0001$) and 99.92% (3.09 log units, $P = 0.022$) were found, while TC-DY-TA performed more modestly with 99.58% (1.61 log units, $P = 0.0007$) inactivation. Overall, our observations here showed that Grampositive *S. aureus* is more susceptible to inactivation than Gram-negative *E. coli*, which is consistent with the literature studies [11, 16, 24–26] on other photodynamic materials that showed that Gram-negative strains, due to their relatively more impermeable outer membrane, are more resistant to in vitro photodynamic inactivation than Gram-positive strains.

3.2.3 Photostability of the dyed antimicrobial fabrics

The photostability of the fabrics was assessed through both color depth (K/S) spectra and photodynamic antimicrobial efficacy. Different light sources and illumination times, i.e., Xe lamp, 500 W, for 12 h (suffix as 'B12h') and white LED light, 10 W, for 5 days (suffix as 'LED'), were employed in the evaluation. Different humidity conditions were also considered as a parameter under xenon lamp illumination (suffix as 'HB12h'). The photodynamic antimicrobial efficacies of the photobleached fabrics against *S. aureus* and *E. coli* were evaluated under the same protocol described above for the dual-dyed TC fabrics. As expected, no notable inactivation was observed for any of the dark control samples of the bleached fabrics (Figure S2). As shown in Fig. 11 (non-bleach vs. B12h) for *S. aureus*, all 'photo-aged' dual-dyed fabrics were less effective than the fresh dual-dyed TC fabrics by ~ 1–2 log units. This resulted in the least effective material possessing a relatively poor inactivation of 88.63% (TC-DB-TA), with the most effective one being relatively good at 98.88% inactivation (TC-DR-TA). Notably, however, the antimicrobial efficacy of the 'photo-aged' TA single-dyed fabric only achieved 71.4% inactivation upon illumination, suggesting that the presence of the disperse dyes protected the dual-dyed fabrics from more extensive photobleaching under the B12h conditions. A similar phenomenon was observed when the fabrics were examined against *E. coli*: TC-TA (B12h) was less effective than pristine TC-TA, reaching only 58% inactivation after 60 min illumination. The inactivation of *E. coli* in the presence of 'photo-aged' dual-dyed fabrics was lower by ~ 1–2 log units when compared to the pristine materials, but with the best material (TC-DB-TA) still able to reach 99.17% inactivation.

To further evaluate the photostability of the fabrics under illumination conditions that better simulate real-life conditions, the fabrics were photo-aged using a more common 10 W white LED light. As shown in Fig. 11, after 5 days of LED photobleaching, the dual-dyed fabrics were less effective than their pristine counterparts, but still achieved 96.54%, 99.24%, 91.79% and 90.33% inactivation with
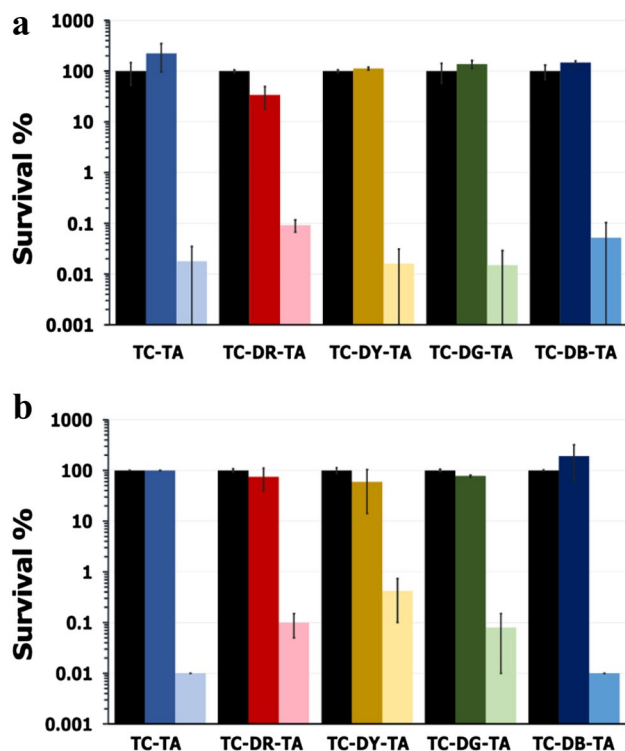
Fig. 10 Photodynamic inactivation studies employing TC-TA (indigo columns), TC-DR-TA (red columns), TC-DY-TA (yellow columns), TC-DG-TA (green columns) and TC-DB-TA (blue columns) against (**a**) *S. aureus* and (**b**) *E. coli*. Displayed are the % survival (vs material-free dark control) for the material-free control (left columns with black color), dark control (middle columns with deeper relative color) and illuminated conditions (right column with lighter relative color). Illumination conditions are the same for all inactivation studies (60 min, xenon lamp at 500 W, equipped with a long-pass filter $\lambda \geq 420$ nm). The detection limits for *S. aureus and E. coli* were 0.001% and 0.01%, respectively
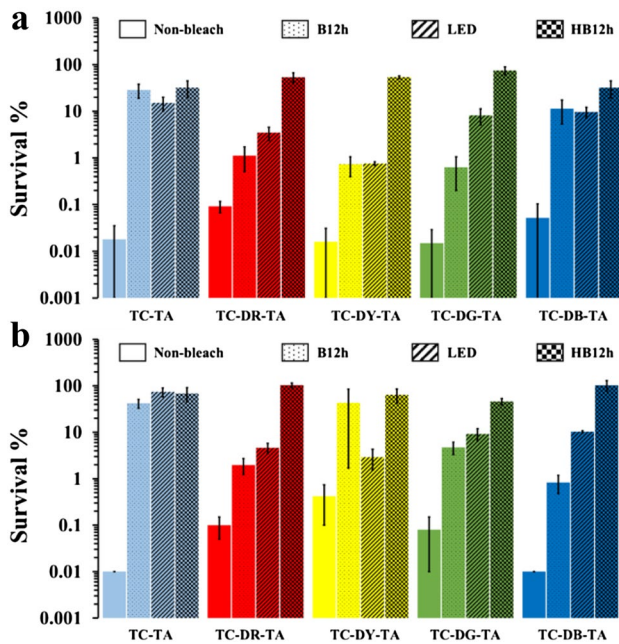
Fig. 11 The % survival (*vs* material-free dark control) of photodynamic inactivation studies performed with pristine fabrics (plain columns), and those that were photobleached under xenon light for 12 h (dotted), LED light for 5 days (diagonal hashes) and xenon light for 12 h with water (checkered) against (**a**) *S. aureus* and (**b**) *E. coli*. Illumination conditions were the same for all inactivation studies [60 min, xenon lamp (500 W) equipped with a long-pass filter ($\lambda \geq 420$ nm)]. The detection limits for *S. aureus* and *E. coli* were 0.001% and 0.01%, respectively

Fig. 12 Antiviral photodynamic inactivation studies employing TC-DR-TA and TC-DG-TA against human coronavirus 229E. Displayed are the material-free dark control (right column), material-present dark controls (middle columns), and material-present light studies (left columns)

TC-DR-TA (LED), TC-DY-TA (LED), TC-DG-TA (LED) and TC-DB-TA (LED), respectively, against *S. aureus*, and 95.38%, 97.08%, 90.77% and 89.75% inactivation against *E. coli*. By way of comparison, TC-TA (LED) exhibited the lowest bactericidal activity among the LED bleached materials of 84.9% inactivation against *S. aureus* and 26% inactivation against *E. coli* when compared to the pristine TC-TA material. Again, these results demonstrate that the presence of the disperse dyes protected the dual-dyed material from more extensive photobleaching under prolonged LED illumination.

Although the photobleaching mechanism of a photosensitizer is complicated, it is widely believed that the ROS produced by the excited PS are themselves responsible for photosensitizer decomposition [52]. As to the protective role of the disperse dyes, two possibilities can be considered: first, that the dispersed dyes absorb light rather than the thionine photosensitizer, leading to less ROS produced (as supported by the DPBF results above), and thereby protecting the photosensitizer from ROS-mediated oxidative damage; or second, the disperse dyes themselves react with the ROS, thus serving as sacrificial substrates in lieu of thionine. Finally, it is known that water can react with an excited state photosensitizer to form hydroxyl radicals
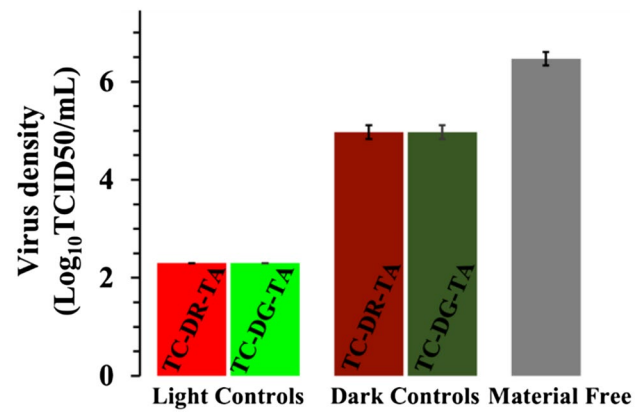
(OH), superoxide (O_2^-) and hydrogen peroxide (H_2O_2), and that these ROS can further accelerate photosensitizer decomposition [53]. To investigate this, water was added to the fabrics during the 12 h xenon illumination studies (HB12h). In all cases, these conditions resulted in less than 1 log unit of pathogen inactivation regardless of the fabric examined or the bacterium studied, thus demonstrating that environmental humidity is an important parameter for the photostability of photodynamic fabrics. Although these data show both single and dual-dyed fabrics were susceptible to photobleaching, they still demonstrated sufficient photostability for applications ranging from disposable to short-term use textiles, particularly under dry conditions.

3.2.4 Antiviral study of TC-DR-TA and TC-DG-TA fabrics

The antiviral photodynamic activities of TC-DR-TA and TC-DG-TA fabrics were evaluated against the enveloped human coronavirus 229E (HCoV-229E) under LumaCare PDT light (60 min, 400–700 nm, 65 ± 5 mW/cm^2). When compared to the material-free dark control that was set to 100% survival (Fig. 12), in the presence of both TC-DR-TA and TC-DG-TA, the dark controls exhibited ~ 1 log unit reduction in virus density, which may be ascribed to an incidental amount of minimal light exposure needed to perform the biological assays or the fouling effect introduced by the fabric samples. Notably, upon illumination (60 min, 400–700 nm, 65 ± 5 mW/cm^2) in the presence of TC-DR-TA or TC-DG-TA, a ~ 99.99% reduction (4.17 log units, $P = 0.0042$) in virus density was observed for both samples. These results confirm that the dual-dyed fabrics are capable of the photodynamic inactivation of enveloped viruses.

4 Conclusions

We successfully prepared dual-dyed PET/cotton blended fabrics with variable color tunability that were capable of the photodynamic inactivation of Gram-positive *S. aureus*, Gram-negative *E. coli* and enveloped HCoV-229E virus. Both the HTHP dyeing and triazine coupling reactions employed in the production of these fabrics resulted in minimal damage to the fabric in terms of their morphologies and mechanical properties, and the thermal properties of the dyed fabric were improved compared to those of the pristine TC fabric. Colorimetric characterization qualitatively demonstrated the successful loading of thionine, with the disperse dyes having the dominant effect on the color expression of the fabrics. CLSM further confirmed the localization of disperse dyes and thionine were mainly on the PET and cotton fibers, respectively. The presence of the disperse dyes did not significantly impact the photodynamic inactivation ability of the thionine photosensitizer, with both Gram-positive *S. aureus* and Gram-negative *E. coli* being photodynamically susceptible to single and dual-dyed thionine-loaded fabrics. Compared to the dual-dyed fabrics, the thionine-only single-dyed TC-TA exhibited poorer photostability under both xenon and LED lights, demonstrating that the disperse dyes afford a measure of protection to the photosensitizer against photobleaching. While humidity was also illustrated as an important factor that has a negative effect on the photostability of the dyed fabrics, measures can be taken to increase fabric hydrophobicity in future iterations of material design. Taken together, these findings suggest that PET/cotton blended fabrics possessing both a photosensitizer for bactericidal/virucidal activity and a disperse dye for color variation have promising applications as easily implementable, yet effective self-disinfecting textiles for PPE that can inhibit the transmission of pathogens based on an irreversible, nonspecific, and nontoxic photodynamic mode of action.

Supplementary Information The online version contains supplementary material available at https://doi.org/10.1007/s43630-023-00398-1.

Declarations

References

1. Scott, R.D. (2009) The direct medical costs of healthcare-associated infections in US hosptials and the benefits of prevention, in, Centers for Disease Control and Prevention, pp. 13.

2. Livingston, E., Desai, A., & Berkwits, M. (2020). Sourcing personal protective equipment during the COVID-19 pandemic. *JAMA, 323*, 1912–1914.

3. Bauchner, H., Fontanarosa, P. B., & Livingston, E. H. (2020). Conserving supply of personal protective equipment—a call for Ideas. *JAMA, 323*, 1911–1911.

4. Borkow, G., Zhou, S. S., Page, T., & Gabbay, J. (2010). A novel anti-influenza copper oxide containing respiratory face mask. *PLoS ONE, 5*, e11295.

5. Kim, Y. K. (2017). 5 - The use of polyolefins in industrial and medical applications. In S. C. O. Ugbolue (Ed.), *Polyolefin Fibres (Second Edition)* (pp. 135–155). Woodhead Publishing.

6. Tomas, M. E., Kundrapu, S., Thota, P., Sunkesula, V. C. K., Cadnum, J. L., Mana, T. S. C., Jencson, A., O'Donnell, M., Zabarsky, T. F., Hecker, M. T., Ray, A. J., Wilson, B. M., & Donskey, C. J. (2015). Contamination of health care personnel during removal of personal protective equipment. *JAMA Internal Medicine, 175*, 1904–1910.

7. Casanova, L., Alfano-Sobsey, E., Rutala, W. A., Weber, D. J., & Sobsey, M. (2008). Virus transfer from personal protective equipment to healthcare employees' skin and clothing. *Emerging Infectious Disease journal, 14*, 1291.

8. Peila, R., Vineis, C., Varesano, A., & Ferri, A. (2013). Different methods for β-cyclodextrin/triclosan complexation as antibacterial treatment of cellulose substrates. *Cellulose, 20*, 2115–2123.

9. Zhang, H., & Oyanedel-Craver, V. (2013). Comparison of the bacterial removal performance of silver nanoparticles and a polymer based quaternary amine functiaonalized silsesquioxane coated point-of-use ceramic water filters. *Journal of Hazardous Materials, 260*, 272–277.

10. Bober, P., Liu, J., Mikkonen, K. S., Ihalainen, P., Pesonen, M., Plumed-Ferrer, C., von Wright, A., Lindfors, T., Xu, C., & Latonen, R. M. (2014). Biocomposites of nanofibrillated cellulose, polypyrrole, and silver nanoparticles with electroconductive and antimicrobial properties. *Biomacromolecules, 15*, 3655–3663.

11. Peddinti, B. S. T., Scholle, F., Ghiladi, R. A., & Spontak, R. J. (2018). Photodynamic polymers as comprehensive anti-infective materials: staying ahead of a growing global threat. *ACS Applied Materials & Interfaces, 10*, 25955–25959.

12. Maldonado-Carmona, N., Ouk, T.-S., Calvete, M. J. F., Pereira, M. M., Villandier, N., & Leroy-Lhez, S. (2020). Conjugating biomaterials with photosensitizers: advances and perspectives for photodynamic antimicrobial chemotherapy. *Photochemical & Photobiological Sciences, 19*, 445–461.

13. Stensberg, M. C., Wei, Q., McLamore, E. S., Porterfield, D. M., Wei, A., & Sepúlveda, M. S. (2011). Toxicological studies on silver nanoparticles: challenges and opportunities in assessment, monitoring and imaging. *Nanomedicine (London, England), 6*, 879–898.

14. Abrahamse, H., & Hamblin, Michael R. (2016). New photosensitizers for photodynamic therapy. *Biochemical Journal, 473*, 347–364.

15. Decraene, V., Pratten, J., & Wilson, M. (2006). Cellulose acetate containing toluidine blue and rose bengal is an effective

antimicrobial coating when exposed to white light. *Applied and Environment Microbiology, 72,* 4436–4439.

16. Alvarado, D. R., Argyropoulos, D. S., Scholle, F., Peddinti, B. S. T., & Ghiladi, R. A. (2019). A facile strategy for photoactive nanocellulose-based antimicrobial materials. *Green Chemistry, 21,* 3424–3435.

17. Dong, J., Ghiladi, R. A., Wang, Q., Cai, Y., & Wei, Q. (2018). Protoporphyrin-IX conjugated cellulose nanofibers that exhibit high antibacterial photodynamic inactivation efficacy. *Nanotechnology, 29,* e265601.

18. Dong, J., Ghiladi, R. A., Wang, Q., Cai, Y., & Wei, Q. (2018). Protoporphyrin IX conjugated bacterial cellulose via diamide spacer arms with specific antibacterial photodynamic inactivation against *Escherichia coli. Cellulose, 25,* 1673–1686.

19. Carpenter, B. L., Scholle, F., Sadeghifar, H., Francis, A. J., Boltersdorf, J., Weare, W. W., Argyropoulos, D. S., Maggard, P. A., & Ghiladi, R. A. (2015). Synthesis, characterization, and antimicrobial efficacy of photomicrobicidal cellulose paper. *Biomacromolecules, 16,* 2482–2492.

20. Carpenter, B. L., Feese, E., Sadeghifar, H., Argyropoulos, D. S., & Ghiladi, R. A. (2012). Porphyrin-cellulose nanocrystals: a photobactericidal material that exhibits broad spectrum antimicrobial activity. *Photochemistry and Photobiology, 88,* 527–536.

21. Feese, E., Sadeghifar, H., Gracz, H. S., Argyropoulos, D. S., & Ghiladi, R. A. (2011). Photobactericidal porphyrin-cellulose nanocrystals: synthesis, characterization, and antimicrobial properties. *Biomacromolecules, 12,* 3528–3539.

22. Stoll, K. R., Scholle, F., Zhu, J., Zhang, X., & Ghiladi, R. A. (2019). BODIPY-embedded electrospun materials in antimicrobial photodynamic inactivation. *Photochemical & Photobiological Sciences, 18,* 1923–1932.

23. Stanley, S., Scholle, F., Zhu, J., Lu, Y., Zhang, X., Situ, X., & Ghiladi, R. (2016). Photosensitizer-embedded polyacrylonitrile nanofibers as antimicrobial non-woven textile. *Nanomaterials, 6,* e77.

24. Peddinti, B. S. T., Morales-Gagnon, N., Pourdeyhimi, B., Scholle, F., Spontak, R. J., & Ghiladi, R. A. (2021). Photodynamic coatings on polymer microfibers for pathogen inactivation: effects of application method and composition. *ACS Applied Materials & Interfaces, 13,* 155–163.

25. Ghareeb, C. R., Peddinti, B. S. T., Kisthardt, S. C., Scholle, F., Spontak, R. J., & Ghiladi, R. A. (2021). Towards universal photodynamic coatings for infection control. *Frontiers in Medicine.* https://doi.org/10.3389/fmed.2021.657837

26. Chen, W., Chen, J., Li, L., Wang, X., Wei, Q., Ghiladi, R. A., & Wang, Q. (2019). Wool/acrylic blended fabrics as next-generation photodynamic antimicrobial materials. *ACS Applied Materials & Interfaces, 11,* 29557–29568.

27. Wang, T., Chen, W., Dong, T., Lv, Z., Zheng, S., Cao, X., Wei, Q., Ghiladi, R. A., & Wang, Q. (2020). Color-variable photodynamic antimicrobial wool/acrylic blended fabrics. *Materials (Basel), 13,* 4141.

28. Wilkinson, F., Helman, W. P., & Ross, A. B. (1995). Rate constants for the decay and reactions of the lowest electronically excited singlet state of molecular oxygen in solution. An EXPANDED AND REVISED compilation. *Journal of Physical and Chemical Reference Data, 24,* 663–677.

29. Dahl, T. A., Midden, W. R., & Hartman, P. E. (1987). Pure singlet oxygen cytotoxicity for bacteria. *Photochemistry and Photobiology, 46,* 345–352.

30. Böhling, A., Bielfeldt, S., Himmelmann, A., Keskin, M., & Wilhelm, K.-P. (2014). Comparison of the stratum corneum thickness measured in vivo with confocal raman spectroscopy and confocal reflectance microscopy. *Skin Res. Technol., 20,* 50–57.

31. Rahimi, R., Fayyaz, F., & Rassa, M. (2016). The study of cellulosic fabrics impregnated with porphyrin compounds for use as photo-bactericidal polymers. *Materials Science and Engineering: C, 59,* 661–668.

32. Castriciano, M. A., Zagami, R., Casaletto, M. P., Martel, B., Trapani, M., Romeo, A., Villari, V., Sciortino, M. T., Grasso, L., Guglielmino, S., Scolaro, L. M., & Mazzaglia, A. (2017). Poly(carboxylic acid)-cyclodextrin/anionic porphyrin finished fabrics as photosensitizer releasers for antimicrobial photodynamic therapy. *Biomacromolecules, 18,* 1134–1144.

33. Chen, W., Wang, W., Ge, X., Wei, Q., Ghiladi, R. A., & Wang, Q. (2018). Photooxidation properties of photosensitizer/direct dye patterned polyester/cotton fabrics. *Fiber Polym., 19,* 1687–1693.

34. El Messiry, M., El Ouffy, A., & Issa, M. (2015). Microcellulose particles for surface modification to enhance moisture management properties of polyester, and polyester/cotton blend fabrics. *Alexandria Engineering Journal, 54,* 127–140.

35. Wang, T., Xu, L., Shen, H., Cao, X., Wei, Q., Ghiladi, R. A., & Wang, Q. (2020). Photoinactivation of bacteria by hypocrellin-grafted bacterial cellulose. *Cellulose, 27,* 991–1007.

36. Piwowar, K., Blacha-Grzechnik, A., & Zak, J. (2015). Photogeneration of singlet oxygen by thionine molecular layer grafted on electrode surface from its diazonium salt. *Electrochemistry Communications, 55,* 10–13.

37. Wang, T., Ke, H., Chen, S., Wang, J., Yang, W., Cao, X., Liu, J., Wei, Q., Ghiladi, R. A., & Wang, Q. (2021). Porous protoporphyrin IX-embedded cellulose diacetate electrospun microfibers in antimicrobial photodynamic inactivation. *Materials Science and Engineering: C, 118,* 111502.

38. Clark, M., (2011). *Handbook of textile and industrial dyeing.* Woodhead Publishing Limited, pp. 116–117.

39. Klemm, D., Heublein, B., Fink, H. P., & Bohn, A. (2005). Cellulose: fascinating biopolymer and sustainable raw material. *Angewandte Chemie, 44,* 3358–3393.

40. Zou, H., Lin, S., Tu, Y., Liu, G., Hu, J., Li, F., Miao, L., Zhang, G., Luo, H., Liu, F., Hou, C., & Hu, M. (2013). Simple approach towards fabrication of highly durable and robust superhydrophobic cotton fabric from functional diblock copolymer. *Journal of Materials Chemistry A, 1*(37), 11246–11260.

41. Mitchell, R., Carr, C. M., Parfitt, M., Vickerman, J. C., & Jones, C. (2005). Surface chemical analysis of raw cotton fibres and associated materials. *Cellulose, 12,* 629–639.

42. Xue, C.-H., Bai, X., & Jia, S.-T. (2016). Robust, self-healing superhydrophobic fabrics prepared by one-step coating of pdms and octadecylamine. *Scientific Reports.* https://doi.org/10.1038/srep27262

43. Kozłowski, R. M., & Mackiewicz-Talarczyk, M. (2020). 1A - Introduction to natural textile fibres. In R. M. Kozłowski & M. Mackiewicz-Talarczyk (Eds.), *Handbook of natural fibres (Second Edition)* (pp. 1–13). Woodhead Publishing.

44. Silva, C., Silva Filho, E., Uliana, F., Jesus, L., De Melo, C. V., Barthus, R., Rodrigues, J., & Vanini, G. (2018). PET glycolysis optimization using ionic liquid [Bmin]ZnCl3 as catalyst and kinetic evaluation. *Polímeros.* https://doi.org/10.1590/0104-1428.00418

45. Neumeyer, J. P., Wadsworth, J. I., Knoepfler, N. B., & Mack, C. H. (1976). Thermogravimetric analysis of polyester/cotton blends treated with Thpc-urea-poly(vinyl bromide). *Thermochimica Acta, 16,* 133–148.

46. Yasin, S., Massimo, C., Rovero, G., Behary, N., Perwuelz, A., Giraud, S., Migliavacca, G., Chen, G., & Guan, J. (2017). An alternative for the end-of-life phase of flame retardant textile products: degradation of flame retardant and preliminary settings of energy valorization by gasification. *BioResources, 12,* 5196–5211.

47. Diaz-Diestra, D., Beltran-Huarac, J., Bracho-Rincon, D. P., Gonzalez-Feliciano, J. A., Gonzalez, C. I., Weiner, B. R., & Morell, G. (2015). Biocompatible ZnS: Mn quantum dots for reactive oxygen

generation and detection in aqueous media. *Journal of Nanoparticle Research, 17*, 461.

48. Huang, L., Xuan, Y., Koide, Y., Zhiyentayev, T., Tanaka, M., & Hamblin, M. R. (2012). Type I and Type II Mechanisms of antimicrobial photodynamic therapy: an in vitro study on gram-negative and gram-positive bacteria. *Lasers in Surgery and Medicine, 44*, 490–499.

49. Wang, W., Zhang, W., Sun, H., Du, Q., Bai, J., Ge, X., & Li, C. (2019). Enhanced photodynamic efficiency of methylene blue with controlled aggregation state in silica-methylene bule-acetate@tannic acid-iron(III) ions complexes. *Dyes Pigments, 160*, 663–670.

50. Dean, J. C., Oblinsky, D. G., Rafiq, S., & Scholes, G. D. (2016). Methylene blue exciton states steer nonradiative relaxation: ultrafast spectroscopy of methylene blue dimer. *The Journal of Physical Chemistry B, 120*, 440–454.

51. Severino, D., Junqueira, H. C., Gugliotti, M., Gabrielli, D. S., & Baptista, M. S. (2003). Influence of negatively charged interfaces on the ground and excited state properties of methylene blue. *Photochemistry and Photobiology, 77*, 459–468.

52. Georgakoudi, I., & Foster, T. H. (1998). Singlet oxygen-versus nonsinglet oxygen-mediated mechanisms of sensitizer photobleaching and their effects on photodynamic dosimetry. *Photochemistry and Photobiology, 67*, 612–625.

53. Pouretedal, H. R., Norozi, A., Keshavarz, M. H., & Semnani, A. (2009). Nanoparticles of zinc sulfide doped with manganese, nickel and copper as nanophotocatalyst in the degradation of organic dyes. *Journal of Hazardous Materials, 162*, 674–681.

Authors and Affiliations

Chenyu Jiang[1] · **Sarah Dejarnette**[2,5] · **Wangbingfei Chen**[3] · **Frank Scholle**[2,5] · **Qingqing Wang**[3] · **Reza A. Ghiladi**[4,5]

✉ Chenyu Jiang
  cjiang@szcu.edu.cn

✉ Qingqing Wang
  qqwang@jiangnan.edu.cn

✉ Reza A. Ghiladi
  Reza_Ghiladi@ncsu.edu

[1] School of Optical and Electronic Information, Suzhou City University, Suzhou, Jiangsu 215104, China

[2] Department of Biological Sciences, North Carolina State University, Raleigh, NC 27695, USA

[3] Key Laboratory of Eco-Textiles, Ministry of Education, Jiangnan University, Wuxi, Jiangsu 214122, China

[4] Department of Chemistry, North Carolina State University, Raleigh, NC 27695, USA

[5] Center for Advanced Virus Experimentation, North Carolina State University, Raleigh, USA